# Asymmetry of electron and hole doping in $YMnO_3$

Bas B. Van Aken, Jan-Willem G. Bos, Robert A. de Groot, and Thomas T. M. Palstra*
*Solid State Chemistry Laboratory, Materials Science Center, University of Groningen, Nijenborgh 4, 9747 AG Groningen, The Netherlands*

(Received 6 October 2000; revised manuscript received 14 December 2000; published 13 March 2001)

We synthesized hexagonal $YMnO_3$ doped with tetravalent Zr ions and studied the electronic and magnetic properties. Zr substitution creates a mixed $Mn^{3+}$-$Mn^{2+}$ system, instead of the conventional $Mn^{3+}$-$Mn^{4+}$ of colossal magnetoresistance manganites. The $YMnO_3$ system displays a pronounced asymmetry for electron and hole doping. Hole doping results in a conducting state, whereas electron doping retains the insulating state. This asymmetry is a consequence of the crystal field splitting of the Mn ions in trigonal bipyramidal coordination.

DOI: 10.1103/PhysRevB.63.125127 PACS number(s): 68.55.Ln

The colossal magnetoresistance compounds based on doped $LaMnO_3$ exhibit metal-insulator transitions that are concurrent with ferromagnetic ordering. The electronic properties are determined by a competition between localization, caused by electron-phonon interaction and on-site Coulomb repulsion, and itinerancy caused by double exchange.[1] The electron-phonon coupling is most apparent from the Jahn-Teller activity of the $Mn^{3+}$ $d^4$ state, which leads to structural distortions that can identify the orbital occupation. Interestingly, there is an asymmetry between hole doping of $LaMnO_3$, $d^4 \rightarrow d^3$, leading to metallicity,[2] and electron doping of $CaMnO_3$, $d^3 \rightarrow d^4$, which remains in an insulating, charge ordered state.[3] The origin of the asymmetry is based on the balance between Jahn-Teller distortion, on-site Coulomb repulsion, and double exchange.

In this paper, we report on the asymmetry of hole and electron doping in the electronic properties of hexagonal $YMnO_3$. In this compound hole doping by $Ca^{2+}$, $d^4 \rightarrow d^3$, results in a conducting state,[4] whereas electron doping by $Zr^{4+}$, $d^4 \rightarrow d^5$, retains the insulating state. This asymmetry can be understood in terms of the orbital occupation dictated by the crystallographic structure. Hole doping results in partial occupation of the $xy$ and $x^2-y^2$ orbitals, which have good overlap, whereas electron doping partially fills the $3z^2-r^2$ orbitals, which have poor overlap.

The influence of doping by tetravalent ions in the manganese perovskites is little studied. Typically, the ionic radius of tetravalent ions is incompatible with that of the trivalent rare earth ions that form the perovskite structure. Therefore, polyvalent elements such as Pb or Ce do not adopt the tetravalent state in $LaMnO_3$.[5] Nevertheless, tetravalent doping would be very significant because it leads to a mixed valence system $d^4$-$d^5$ instead of the conventional $d^4$-$d^3$ system. The higher spin value of $d^5$ could lead to higher magnetic ordering temperatures, while preserving the strong electron-phonon interaction of the Jahn-Teller active $d^4$ $Mn^{3+}$ ions.

In order to stabilize $LaMnO_3$ including tetravalent ions, small rare earth ions are required to minimize the variance of the ionic size. We have found that a large ionic size mismatch, such as between $La^{3+}$ and $Zr^{4+}$, results in phase separation. Therefore, we choose $Y^{3+}$, being somewhat larger than $Zr^{4+}$. While $YMnO_3$ can be synthesized in the orthorhombic *Pnma* structure,[6–8] we focus here on the hexagonal structure, which is thermodynamically stable for $RMnO_3$ with $R$ a small rare earth ion.[9] The hexagonal structure consists of $MnO_5$ trigonal bipyramids. The bases of the pyramids are corner linked to form a triangular lattice in the $ab$ basal plane. Between these $MnO_5$ sheets, the Y ion is located above the linking oxygens. Each consecutive layer of $MnO_3$ is rotated by 180° along the $c$ axis. $YMnO_3$ is of current technological interest, because of its ferroelectric properties with $T_c \sim 900$ K.[10] Its layered crystal structure is compatible with thin film growth techniques. The ferroelectric component is perpendicular to the layers and can thus be modulated by an external electrical field.

The $YMnO_3$-$ZrMnO_3$ solid state solutions were prepared by mixing pure, dehydrated $Y_2O_3$, $ZrO_2$, and $MnO_2$ in the appropriate stoichiometric amounts. The oxides were repeatedly ground, pressed to pellets, and heated to 1073–1673 K until no change in the diffraction patterns could be seen. Single crystals of $YMnO_3$ were grown from a mixture of $Y_2O_3$ and $MnO_2$ with an approximately 1:12 $Bi_2O_3$ flux in a Pt crucible. Two methods for crystal growth were applied.[11] Resistivity measurements were done in a standard four-contact setup, using a Keithley 236 instrument. This limits the measurable range to 10 GΩ for two-point resistance. Magnetization is measured using a Quantum Design MPMS magnetometer. Single crystals were glued to a clean, glass rod. The perpendicular and parallel settings were achieved by orienting the planes of the platelets parallel and perpendicular to the rod, respectively.

Diffraction patterns of powder samples are obtained on a Philips PW1820 Bragg-Brentano diffractometer with secondary monochromator, using either Cu $K\alpha$ or Mo $K\alpha$ radiation. The patterns were analyzed with the GSAS software package.[12] The Rietveld refinement included profile parameters and sample height correction. We show in Fig. 1 the refined lattice parameters versus the nominal doping level. The lattice parameters $a$ and $c$ both decrease gradually with increasing Zr concentration, but the slope changes significantly above $x=0.3$. Rietveld refinement[12] of the x-ray diffraction (XRD) patterns was carried out to investigate both the doping dependencies of the atomic coordinates and possible mixed site occupancy. The refinement of the fractional coordinates of the ions gave no dependence on the substitution within the error bars. Models involving mixed site oc-

 

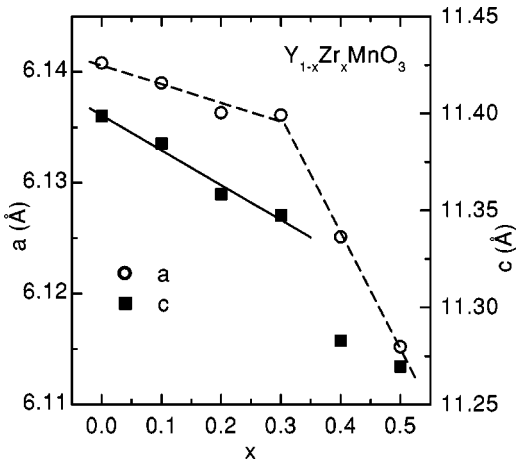


FIG. 1. Lattice parameters of $h$-$Y_{1-x}Zr_xMnO_3$ versus the Zr doping level $x$. Error bars are smaller than the symbol size. For $x < 0.3$ no mixed Mn-Zr site occupancy is observed.

cupancy show that for $x$ up to 0.3 no unwanted mixing is present. However, the refinements of the samples with $x=0.4$ and $x=0.5$ improved significantly, resulting in 40% and 50% of Zr on the Mn site, respectively.

In the literature $YMnO_3$ is reported to order antiferromagnetically at $\sim 80$ K, but no temperature dependent properties are reported.[13] Our magnetization data on ceramic $YMnO_3$ are dominated by a ferromagneticlike ordering at 42 K. No sign of the antiferromagnetic ordering at $\sim 80$ K was observed. In Fig. 2, we show the temperature dependence of the magnetization of $YMnO_3$ single crystals. An antiferromagnetic ordering can be observed at 75 K for the basal plane both parallel and perpendicular to the applied magnetic field. The susceptibility for $H_\perp$ is higher than for $H_\parallel$, where $\perp$ and $\parallel$ refer to orientations with respect to the $ab$ plane. The antiferromagnetic ordering cannot be observed in our ceramic samples, because of the few percent impurity phase of the ferrimagnetic spinel $Mn_3O_4$ with $T_c \sim 42$ K.[14] The high temperature data for the ceramic $YMnO_3$ show a linear dependence between the inverse susceptibility and the temperature. A fit to the Curie-Weiss law yields a Weiss temperature of $-254$ K and an effective moment of $4.5\mu_B$, somewhat

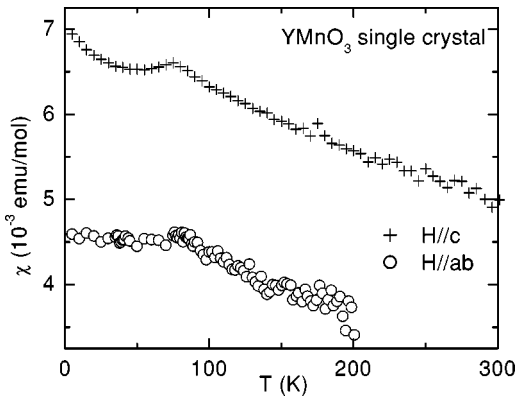


FIG. 2. Temperature dependence of the dc magnetic susceptibility of single crystalline $YMnO_3$ with the external field parallel (+) and perpendicular (○) to the $c$ axis.

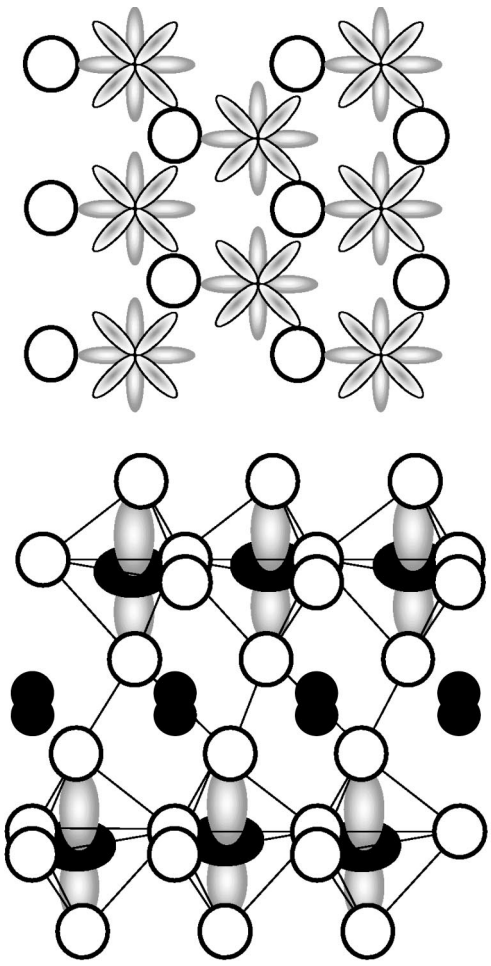

FIG. 3. Sketch of the hexagonal structure of $YMnO_3$. The top panel is a cross section of the $ab$ plane, showing one MnO layer. The bottom panel is a cross section along the $c$ axis, showing the layered nature of this compound. The O ions are represented by open circles; the La ions as striped circles. The Mn ions are represented by their $d$ orbitals. The fully occupied $xy$ and $x^2-y^2$ orbitals and the empty $3z^2-r^2$ orbitals are shown in the top and the bottom panel, respectively. Note the very poor overlap between two consecutive MnO layers.

smaller than the spin-only value expected for $Mn^{3+}$ ions, $4.90\mu_B$.

The crystal structure of the single crystals was determined by x-ray diffraction and is isomorphous with $LuMnO_3$.[9] A schematic view of the structure, showing the pseudolayered nature of these crystals, is shown in Fig. 3. Details of this investigation are published elsewhere.[15] In $YMnO_3$ the Mn-O distances along the $c$ axis as well as in the $ab$ plane are more similar than in $LuMnO_3$. The ferroelectric moment, based on the structure refinement, of $YMnO_3$ is smaller than that of $LuMnO_3$.

The ferroelectric properties originate from the noncentrosymmetric oxygen surroundings of the metal ions. The Mn ions are shifted in the $ab$ plane, resulting in a triangular frustrated displacement. However, the displacement parallel to the $c$ axis of all six Mn ions in the unit cell, with respect to the center of the trigonal bipyramid, is equal. Also, the Y

ions have displacements along the *c* axis; four displacement vectors point up, the other two down. Our structure refinement indicates that the net polarization in zero external field is canceled through inversion twinning.

Electron doping of $YMnO_3$ with Zr results in a mixed valence state of $Mn^{2+}$-$Mn^{3+}$ instead of the conventional $Mn^{3+}$-$Mn^{4+}$ of the colossal magnetoresistance materials. This results in a larger spin state for the Mn, which we expect to enhance $T_c$. We note that the $Mn^{2+}$-$Mn^{3+}$ mixed valence state preserves the double exchange mechanism between $d^4$ and $d^5$ and the strong coupling to the lattice through the Jahn-Teller active $d^4$ ($Mn^{3+}$) ion. We attempted to stabilize this phase by using tetravalent dopants instead of the conventional divalent alkaline earth ions. A number of tetravalent ions adopt a divalent state in the manganite perovskite, such as Pb. In addition, we found that the tetravalent ion Th forms a large number of La-Th mixed oxides. Therefore, we chose Zr as tetravalent dopant.

Although the tolerance factor $t=(\langle r_{A^{2/3+}}\rangle + r_{O^{2-}})/(r_{Mn^{4/3+}} + r_{O^{2-}})$ based on the radii of $La^{3+}$, $Mn^{3+}$, and $Zr^{4+}$, is within the existence range of the orthorhombic structure, doping of $LaMnO_3$ with Zr was unsuccessful, as Zr precipitates as $ZrO_2$. Apparently the tolerance factor alone does not account for the stability regime of the perovskites. It is known that both the average ionic radius and the size difference, or variance $\sigma$, control the properties[16,17] of perovskites. From these doping experiments, we conclude that not only the average values of the ionic radii but also the variance control the stability and existence range. In order to reduce the variance of the ionic radii a much smaller lanthanide was necessary, to enable Zr substitution on the lanthanide site.

It is known that the perovskite structure is stable down to a structure factor of $t=0.85$ for samples with $\sigma=0$.[9] The hexagonal structure is stable under standard synthesis conditions for samples with $t<0.85$. For samples with $\sigma>0$, e.g., $Gd_{1-x}Y_xMnO_3$, the hexagonal structure is stable at higher values than $t=0.8517$.[18] We chose to synthesize and dope $YMnO_3$ with Zr to ensure that our compounds would be hexagonal for all Zr doping levels. With $r_{Zr^{4+}}=0.89$ Å and $r_{Y^{3+}}=1.075$ Å this gives $0.85>t>0.82$ for doping levels up to $x=0.3$.

Increasing the amount of $Zr^{4+}$ substituting for $Y^{3+}$ in $YMnO_3$ results in a clear decrease of the lattice parameters. This means that Zr is incorporated in the crystal structure. For the samples with $x<0.3$, no traces of other Zr containing oxides could be found with either XRD or energy-dispersive spectroscopy. The refinement of the occupation of the Mn site shows that Zr has not replaced Mn in the lattice. Furthermore, substituting for Mn with Zr would most likely increase the lattice parameters, as $Zr^{4+}$ is larger than $Mn^{2+}$. Therefore, we conclude that we introduced tetravalent zirconium in the hexagonal form of $YMnO_3$.

Figure 2 shows the antiferromagnetic ordering in single crystals of $YMnO_3$. From earlier neutron diffraction experiments, it is known that the spins are oriented in the *ab* plane. This agrees with the anisotropy of $\chi$ with $\chi_\perp > \chi_\parallel$. We observe that $\chi_\parallel$ does not go to zero for $T\rightarrow 0$, as expected for a conventional antiferromagnet, but remains finite. The value of $\chi_\parallel$ can be ascribed to the in-plane response of the triangular frustrated magnetic structure as observed by neutron diffraction.[11] Due to the triangular spin structure of these compounds, $\chi_\parallel$ always probes a contribution of the spins perpendicular to the applied magnetic field.

Measurement of the magnetization of powder samples shows ferromagnetic ordering at 42 K. However, the value of the magnetic moment is too low to suggest ferromagnetic or ferrimagnetic ordering of all Mn moments. This behavior is often seen in powder samples of $YMnO_3$.[14] It was concluded that the magnetic transition originates from $Mn_3O_4$ impurities. $Mn_3O_4$ is ferrimagnetic with a spin of $S=2$ (or $4\mu_B$) per formula unit. This suggests that the ceramic $YMnO_3$ sample has a $Mn_3O_4$ impurity of 4 at. %.

The Mn-O bonds in the *ab* plane form a trigonal network. Each oxygen ion links three Mn ions, and each Mn ion is surrounded, in plane, by three oxygens. The superexchange interaction between the Mn ions is antiferromagnetic. However, two neighboring Mn ions share one other Mn ion as nearest neighbor. This results in a frustrated configuration in the planes. The coupling between the layers is much weaker as the superexchange occurs via two oxygens. The large difference between the Weiss temperature $\theta=-254$ K and $T_N=75$ K is attributed to the pseudo-two-dimensional character of this compound and to the frustration. The Weiss temperature signals strong antiferromagnetic coupling and $T_N$ is a measure of the long range magnetic order.

In contrast to Ca doping of *h*-$YMnO_3$,[4] we observe upon Zr doping no measurable increase in the conductivity. All samples had two-point resistances of the order of 1 GΩ or higher at room temperature, near the limit of our measurable range. In order to explain the different effects of electron and hole doping for the electronic conductivity, we calculated the crystal field splitting of the Mn $3d$ orbitals. We assume a simplified structure: Mn surrounded by a perfect equidistant trigonal bipyramid of oxygen ligands. We found a splitting of the $3d$ orbitals into three states. Since the crystal field in the trigonal bipyramid does not contain off-diagonal terms, the splitting is according to the absolute value of the magnetic quantum number. Consequently, the $e_g$ orbitals $x^2-y^2$ and $3z^2-r^2$ are not degenerate as in the orthorhombic perovskites, but $x^2-y^2$ is degenerate with $xy$. The orbitals are filled assuming strong Hund's rule coupling. Both the $xz$ and $yz$ orbitals, which are directed between the oxygens, and the in-plane orbitals $xy$ and $x^2-y^2$ are singly occupied in $YMnO_3$, $Mn^{3+}$ ($3d^4$), whereas the orbital pointing to the two apical oxygens is empty.

Crystal field splitting of *d* levels can be interpreted as the result of a covalent interaction between metal *d* states and anion *p* states. Since the metal d states are usually higher in energy, the states of major *d* character form the antibonding states. The interaction increases with increasing energy and therefore the amount of anion *p* admixture also increases with increasing energy. Thus in a highly symmetrical structure the *d* bands derived from the crystal field split *d* states show a larger bandwidth the higher they are in energy.

In $YMnO_3$, the situation is more complicated. The lowest *d* band is quite localized, while the second band shows more dispersion. The highest *d* state (of $z^2$ character) is fairly lo-

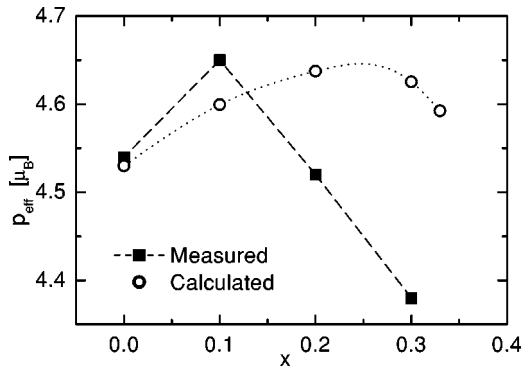


FIG. 4. Magnetic moment as a function of the Zr concentration.

calized again, contrary to the usual situation. In this structure, the weak O-O interaction in the $z$ direction limits the bandwidth, rather than the Mn-O interaction. As a consequence, doping the $d^4$ system with holes has a large effect on the conductivity[4] since the charge carriers are introduced in the dispersive $x^2-y^2$, $xy$ band. However, electron doping leads to occupation of localized majority $z^2$ states and/or localized minority $xz,yz$ states.

The fate of the electrons introduced by Zr substitution can be determined by investigating the size of the magnetic moment as a function of Zr concentration (Fig. 4). The sample with $x=0.1$ shows an increase in the magnetic moment of $0.1\mu_B$, indicating that the extra electrons occupy the majority $3z^2-r^2$ states. An increase in doping to $x=0.2$ leads to a decrease in the magnetic moment. Thus with increased doping minority $xz$ and $yz$ states are occupied. The sample with $x=0.3$ shows a further reduction of magnetic moment. In Fig. 4 the calculated values for the magnetic moment are reported using the *LSW* method in the virtual crystal approximation. Since the size of the magnetic moment in these systems is not expected to be very dependent on the type of magnetic ordering, a simple ferromagnetic structure was assumed. The calculations show a similar trend but the decrease in magnetic moment is less than observed experimentally. The point at $x=0.33$ doping refers to a calculation not employing the virtual crystal approximation but replacing 1/3 of the Y by Zr. Since the value of the magnetic moment obtained in this calculation follows the trend of the values for smaller doping, the virtual crystal approximation is not responsible for the small deviations between theoretical and experimental results.

In this simplified picture, we do not have a strong electron-phonon coupling via the Jahn-Teller effect on the $d^4$ ions, as they have completely filled subbands. Furthermore, the $d^4-d^5$ mixed valence system has no degenerate partially filled orbitals, so electron-phonon coupling via a Jahn-Teller-like distortion cannot occur. In contrast, the $d^3$ ion, with the equidistant, trigonal bipyramidal environment, does have a degeneracy that can be lifted by a structural deformation of the bipyramid. This warrants a direct comparison of $h$-$(Y,Ca)MnO_3$ with the orthorhombic manganites.

We successfully doped hexagonal $YMnO_3$ with tetravalent Zr ions, thereby creating a mixed $Mn^{3+}$ and $Mn^{2+}$ system. This system displays a pronounced asymmetry for electron and hole doping. Hole doping results in a conducting state because of partial occupation of the dispersive $xy$ and $x^2-y^2$ band. Both majority and minority bands are partially occupied by electron doping. However, this remains an insulating state because of the poor overlap of the $3z^2-r^2$ orbitals and the low mixing of the $xz,yz$ band with the O $2p$ orbitals.

This work was supported by the Netherlands Foundation for Fundamental Research on Matter (FOM).

*Email address: Palstra@chem.rug.nl

[1] A.J. Millis, P.B. Littlewood, and B.I. Shraiman, Phys. Rev. Lett. **74**, 5144 (1995).
[2] P. Schiffer, A. Ramirez, W. Bao, and S.-W. Cheong, Phys. Rev. Lett. **75**, 3336 (1995).
[3] J. Hejtmánek, Z. Jirák, M. Marysko, C. Martin, A. Maignan, M. Hervieu, and B. Raveau, Phys. Rev. B **60**, 14 057 (1999).
[4] C. Moure, M. Villegas, J. F. Fernandez, J. Tartaj, and P. Duran, J. Mater. Sci. **34**, 2565 (1999).
[5] R. M. Kusters, J. Singleton, D. A. Keen, R. McGreevy, and W. Hayes, Physica B **155**, 362 (1989).
[6] H. Brinks, H. Fjellvg, and A. Kjekshus, J. Solid State Chem. **129**, 334 (1997).
[7] P.A. Salvador, T.-D. Doan, B. Mercey, and B. Raveau, Chem. Mater. **10**, 2595 (1998).
[8] A. Waintal and J. Chenavas, Mater. Res. Bull. **2**, 819 (1967).
[9] H.L. Yakel, W. Koehler, E.F. Bertaut, and E.F. Forrat, Acta Crystallogr. **16**, 957 (1963).
[10] G. Smolenskii and I. Chupis, Usp. Fiz. Nauk **136–138**, 415 (1982) [Sov. Phys. Usp. **25**, 475 (1982)].
[11] E.F. Bertaut, E.F. Forrat, and P. Fang, C. R. Hebd. Seances Acad. Sci. **256**, 1958 (1963).
[12] R. Von Dreele and A. Larson, Computer code GSAS (Los Alamos National Laboratory, Los Alamos, 1998).
[13] W. Koehler, H.L. Yakel, E. Wollan, and J. Cable, Phys. Lett. **9**, 93 (1964).
[14] E.F. Bertaut, R. Pauthenet, and M. Mercier, Phys. Lett. **18**, 13 (1965).
[15] B. B. Van Aken, A. Meetsma, and T. T. M. Palstra, Acta Crystallogr., Sect. C: Cryst. Struct. Commun. (to be published 1 March 2001).
[16] L.M. Rodríguez-Martnez and J.P. Attfield, Phys. Rev. B **54**, R15 622 (1996).
[17] F. Damay, C. Martin, A. Maignan, and B. Raveau, J. Appl. Phys. **82**, 6181 (1997).
[18] J. W. G. Bos, B. B. Van Aken, and T. T. M. Palstra (unpublished).